Three-Dimensional Finite Element Method Analysis of Turbulent Flow over Self-Propelled Slender Bodies

Russell H. Thomas* and Joseph A. Schetz†
Virginia Polytechnic Institute and State University, Blacksburg, Virginia 24061
and
Dominique H. Pelletier‡
Ecole Polytechnique, Montreal, Quebec, Canada

The three-dimensional Reynolds-averaged Navier-Stokes equations are solved by a finite element method for three slender body conditions. The propeller is modeled by an actuator disk. A zonal turbulence model is used: an integrated turbulent, kinetic energy model in the core of the flow, a mixing-length formulation in the outer region, and a Prandtl wake model downstream of the strut. The turbulence model is incorporated into a modified version of the finite element code FIDAP. Predictions compare very favorably with wind tunnel experiments for the three conditions: self-propelled, 100% overthrust, and propulsion from an ideal-rotor. The swirl was better predicted than previous attempts at this problem. The multilayer turbulence model was essential to proper prediction of the main features of the flow.

Nomenclature

a_2, c_2 = constants in turbulence model
b = width of planar wake
D_0 = diameter of body and of propeller
k = turbulent kinetic energy
L = length scale
l_m = mixing length
Q = torque
R = radius of body and of propeller
T = thrust
U_0 = freestream velocity
ϵ = viscous dissipation
γ = distribution function
ν_T = turbulent eddy viscosity
ρ_0 = freestream density
η = propeller efficiency

Introduction

TURBULENT free shear flows are of great practical importance in many engineering applications, such as mixing and injection flows,[1] and in many propulsion problems. This study focuses on the flow over a propeller-driven body with appendages.

This complex problem has been the subject of several experimental studies[2-9] and can be further complicated by flow stratification and operation at pitch and yaw angles. The ability to predict such flow is crucial to the proper determination of the performance of submarines and pusher-propeller aircraft, for example. Factors such as propeller inflow profiles, thrust deduction, wake dissipation, and hull surface pressures are of interest to the design of many vehicles.

Schetz et al.[11-14] solved the vorticity stream function form of the Navier-Stokes equations using a finite-difference procedure. Predictions compared well for the axial velocity but swirl, although qualitatively correct, was consistently underpredicted.

Pelletier and Schetz[10] introduced a finite element method to solve turbulent three-dimensional flows with propellers. The algorithm proved to be robust and stable due to full coupling of the momentum and continuity equations. Predictions showed excellent agreement with experiments and provided the first predictions of pressure.

The method was later extended to treat a more complicated screen-propeller combination. The screen, located upstream of the rotor, produced a shear flow resembling that of the wake of a body with an appendage. Axial velocity predictions were excellent. However, the quality of swirl calculations decreased somewhat. The research presented here is an extension of that of Refs. 10 and 15 to propeller-driven slender bodies.

Solution Procedure

Experimental Conditions

The present calculations are compared to the experiments of Mitra et al.[16] for turbulent flow over an axisymmetric body supported by a vertical flat plate strut. The body had a length of 2.28 m and a diameter of 0.152 m, resulting in a slenderness ratio of 15. The flat plate was connected to a strain gauge balance to measure drag and yaw moment. A 3-hp motor driving a 3-bladed propeller (0.152 m diameter) provided propulsion. Self-propulsion and overthrust were achieved at rotational speeds of 12,900 and 17,100 rpm, respectively. The Reynolds number based on the body diameter was 4.5×10^5 for a freestream velocity of 47.85 m/s and a density of 1.1277 kg/m^3.

The strut wake and body boundary layer, 1.804 diameters upstream of the propeller, were measured in a separate set of experiments.[17] This location was sufficiently far upstream to be free of any propeller influences. These measurements were used as boundary conditions for the present calculations.

Derivation of Thrust and Torque

For the calculations, values of net thrust and torque produced by the propeller were needed. Unfortunately, from the experiments, only the rpm and the fact that the experiment was self-propelled or at 100% overthrust were known. Also, without the propeller operating, the drag coefficient of the body and strut was measured as 0.25.

Presented as Paper 88-3089 at the AIAA/ASME/SAE/ASEE 24th Joint Propulsion Conference, Boston, MA, July 11-13, 1988; received Aug. 4, 1988; revision received Dec. 11, 1989.

*Research Associate, Aerospace and Ocean Engineering Department. Member AIAA.
†W. Martin Johnson Professor and Department Chairman. Fellow AIAA.
‡Applied Mathematics Department; also Adjunct Professor Aerospace and Ocean Engineering. Member AIAA.

The pressure distribution on the body is changed by the propeller in operation; therefore, a thrust deduction fraction must be added to the drag coefficient of 0.25. The coefficient of drag of 0.25 produces a thrust in the absence of interaction of 6.0 N. Following the method of Ref. 18, the augmented thrust was calculated. The wake fraction was calculated from the axial velocity distribution at the propeller location without the propeller operating. Together with the thrust disk loading coefficient, the thrust deduction fraction is calculated to be 0.098. The augmented thrust with the propeller operating, T, can then be calculated as 6.66 N.

With no direct information on the efficiency of the propeller available, a value of 70% was taken as a typical value for this type of propeller,[19] and torque was calculated as $Q = TU_0/2\pi n\eta$, where n = rps. Torque for the self-propelled case was calculated at 0.349 Nm. Likewise for the 100% overthrust case, thrust was calculated at 13.344 N and torque at 0.509 Nm. The efficiency was assumed to remain at 70%.

Equations of Motion

The full Reynolds-averaged Navier-Stokes equations are used in the simulation and are written in the following form:

$$U_{i,i} = 0 \tag{1}$$

and

$$\rho U_j U_{i,j} = -P_{,i} + \rho f_i + [(\mu + \mu_T)(U_{i,j} + U_{j,i})]_{,j} \tag{2}$$

The laminar viscosity μ is usually several orders of magnitude smaller than the turbulent viscosity μ_T and can often be neglected. In order to close the system, the eddy viscosity and the body forces representing the effects of the propeller must be specified.

The preceding equations of motion along with the turbulence model and propeller body force model, yet to be described, are solved by the finite element method (FEM) in a procedure previously used.[10,15]

The actual Fortran code used to solve the FEM formulation on the incompressible flow problem of interest here is a modified version of the excellent, general-purpose code FIDAP by Fluid Dynamics International.[20,21]

Modeling of the Propeller

The propeller is modeled as a disk of radius and thickness equal to the propeller. Thrust and torque are allowed to vary in the radial direction only. Since the actual thrust and torque distribution is not known, a simple trapezoidal distribution is used. This function is zero for a radius less than $0.0834R$, increases linearly to its maximum value at $0.494R$, remains at this maximum until $0.925R$, and then decreases linearly to zero at the blade tip. This distribution is used for both thrust and torque following its successful use in previous work.[10,15]

Turbulence Model

The present body-propeller combination presents a challenge in turbulence modeling. This is due to the interaction of several distinct turbulent layers. The turbulent boundary layer on the body impinges on the propeller resulting in a combination of jet-wake features. A further complication is the turbulent wake from the strut that will interact with the previously mentioned features. A composite model is adopted to handle all these features.

The integrated turbulence kinetic energy (TKE) model of Refs. 10 and 15 proved very successful for free shear flows around propellers and forms the core for a model of the turbulent mixing in the inner layer downstream of the propeller. A mixing length is used in the outer layer region surrounding the core of the propeller-wake flow. Finally, since the wake of the strut exhibits significant differences when compared to the propeller jet flow, a Prandtl Planar Wake Model is used downstream of the strut.

Inner Layer Integrated Turbulence Kinetic Energy Model

Turbulence in the core flow is modeled using the integrated TKE model of Refs. 10 and 15. The integral form of the TKE equation is obtained by integration over the cross section normal to the mainflow direction:

$$\frac{\mathrm{d}\iint_A \rho U k \,\mathrm{d}A}{\mathrm{d}x} = \int\int_A \nu_T[(U_{,y})^2 + (U_{,z})^2 + (V_{,z} + W_{,y})^2]\,\mathrm{d}A + \int\int_A \epsilon \mathrm{d}A \tag{3}$$

The TKE is related to the eddy viscosity through the Prandtl-Kolmogorov relationship[22]:

$$\nu_T = c_2 k^{1/2} L \tag{4}$$

while dimensional consistency dictates the following form for the viscous dissipation:

$$\epsilon = \frac{a_2 k^{3/2}}{L} \tag{5}$$

To assure boundedness of the integrals in Eq. (3), a distribution function is introduced[10,15] to approximate the form of μ_T across the layer. This function is closely related to the intermittency of the flow[1,23]:

$$\gamma = \gamma_y \gamma_z \tag{6}$$

where

$$\gamma_y = 0.5\left[1 - \mathrm{erf}(3.3232\frac{Y}{Y_{0.9}} - 3.422)\right] \tag{7}$$

and γ_z is written in a similar fashion. Here, $Y_{0.9}$ is the width of the shear layer on the y axis and is defined by the points where

$$\frac{U_{\max} - U_{\text{width}}}{U_{\max} - U_{\min}} = 0.9 \tag{8}$$

Here, $U_{\max}$ is the maximum velocity in the y-z cross plane of interest, $U_{\min}$ is the minimum velocity within the inner layer, and U_{width} is the velocity at the 0.9 width location.

It was felt that the choice of $U_{\max}$ was more appropriate than the half-width. The use of the distribution function results in the following form of the eddy viscosity:

$$\nu_T(x,y,z) = \gamma(y,z) \times \mu_T(x) \tag{9}$$

which produces a sharp drop in eddy viscosity near the width of the inner layer.

The following ordinary differential equation (ODE) is obtained for the eddy viscosity:

$$\frac{\mathrm{d}\nu_T}{\mathrm{d}x} = 0.5\left(\frac{Y_2 - \dfrac{\nu_T \mathrm{d}Y_1}{\mathrm{d}x} - \nu_T^2 Y_3}{Y_1}\right) \tag{10}$$

where

$$Y_1 = \int\int_A \frac{\rho U \gamma^2}{c_2 L^2}\,\mathrm{d}A \tag{11}$$

$$Y_2 = \int\int_A \gamma[(U_{,y})^2 + (U_{,z})^2 + (V_{,z} + W_{,y})^2]\,\mathrm{d}A \tag{12}$$

and

$$Y_3 = \int\int_A \frac{\gamma a_2}{c_2^3 L^4}\,\mathrm{d}A \tag{13}$$

Y_1, Y_2, and Y_3 are the convection, production, and dissipation integrals. The dissipation length scale is computed as[24,25]

$$L = \left[\frac{(Y_{0.9}^a Z_{0.9}^a)}{(Y_{0.9}^a + Z_{0.9}^a)} \right]^{1/a} \tag{14}$$

This insures proper transition from planar to axisymmetric flows in three dimensions.

Finally, an initial condition must be supplied for the initial value problem, Eq. (9). This value of the nondimensional eddy viscosity was estimated at 0.000454 from the turbulence measurements at the inflow plane.[17]

The model was calibrated on the far-field solution for a round jet.[26,27] The eddy viscosity is constant; hence, the left-hand side of Eq. (9) is zero, and all integrals are easily evaluated. Balance between production and dissipation leads to $a_2 c_2 = 0.08$.[28] The solution of Eq. (9) yields $a_2 = 1.0345$ and $c_2 = 0.0773$. See Ref. 10 for more details.

The integrated TKE model was originally developed for free shear layers. However, with modifications, it was used for an approximate treatment of the wall boundary layer for the reason of complexity vs benefit. It was felt that the propeller would dominate the wake and be unaffected by the details of the innermost layer of the surface boundary layer. Furthermore, prediction of skin friction on the surface was not of direct interest here. The first modification was to fix the TKE production to zero at the wall node. Second, following Clauser,[29] a slip velocity was imposed at the wall to produce reasonable values of skin friction on the body. At the inflow, a large slip velocity was needed to produce a skin friction coefficient of 0.003. The slip velocity was smoothly decreased down the body to achieve the observed value of 0.001 for the skin friction.

Outer Layer Model

The outer layer is located radially out from the velocity peak due either to the wall boundary layer or the propeller. Eddy viscosity is formulated in terms of a mixing length:

$$\mu_T = \rho l_m^2 \left| \frac{\partial u}{\partial r} \right| \tag{15}$$

where l_m is the mixing length given by

$$l_m = 0.125 \text{ (width of the outer layer)} \tag{16}$$

The constant 0.125 is taken from Ref. 30, and the width of the outer layer is determined in a manner consistent with the inner layer widths.

Planar Wake Model

Prandtl's planar wake model[31] was chosen for the wake of the flat plate strut:

$$\mu_T = 0.037 b_{1/2} \left| U_{\max} - U_{\min} \right| \tag{17}$$

where the half-width is simply the width at the velocity that is the average of $U_{\max}$ and $U_{\min}$. From the experimental profiles at the inflow plane, the eddy viscosity was calculated at several cuts across the planar wake and found to be approximately constant.

The growth of planar wakes is well predicted by a similarity analysis found in Ref. 32:

$$b_{\text{planar}} = 0.057 (x C_D D)^{1/2} \tag{18}$$

The eddy viscosity is computed throughout the domain using the appropriate model. The effective viscosity is given by the addition of the turbulent eddy viscosity μ_T and the laminar viscosity μ_L. The laminar viscosity must be included since μ_T can reach near zero values in parts of the domain. A dimensionless value of 10^{-4} was used for μ_L.

Results

Three three-dimensional simulations were performed. The baseline case corresponds to the self-propelled condition of Ref. 16. For the overthrust case, thrust and torque were increased 100% over the baseline case. A no-swirl case was also calculated corresponding to an ideal rotor-stator arrangement having the same thrust as that of the baseline case.

Grid Requirements

Finite element simulations of three-dimensional incompressible flows are very expensive. Reduction of both extent of the mesh and number of grid points results in significant computational savings. In order to determine minimal grid requirements, a series of two-dimensional axisymmetric simulations were performed.

A grid independent reference solution was obtained on a large flow domain using a very fine grid. The grid was then coarsened and the domain reduced in successive steps. For each grid, the solution was compared to the benchmark to insure that the quality of predictions did not deteriorate. The final grid extends from $1.804D$ upstream of the propeller to $2D$ downstream and from the axis radially $1D$. The grid contains 15 and 24 nodes in the radial and streamwise directions, respectively.

The three-dimensional grid was obtained by spinning the two-dimensional mesh around the axis. A total of 16 planes are used in the peripheral directions. The resulting mesh contained 5625 nodes and 5152 eight-noded bricks. Figure 1 shows a longitudinal cut through the mesh, and Fig. 2 provides a perspective view. Note the refinement near the propeller and in the wake regions.

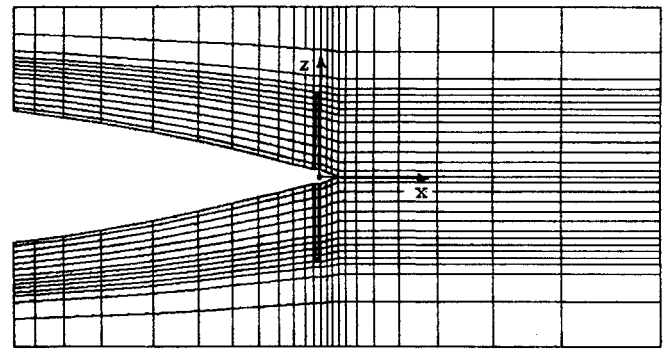

Fig. 1 Longitudinal cut through the three-dimensional grid; propeller is outlined.

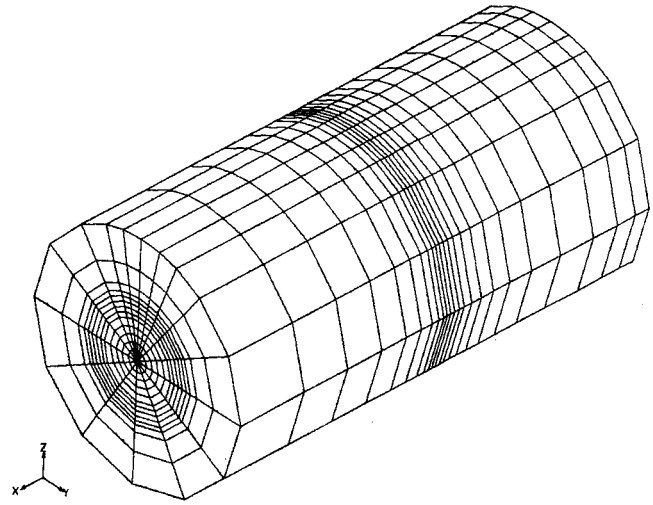

Fig. 2 Full view of three-dimensional grid.

Table 1 Computing statistics

Case	CPU, h	Cost, dollars
Baseline	9.66	2100
Overthrust	12.33	2650
No-swirl	2.28	520

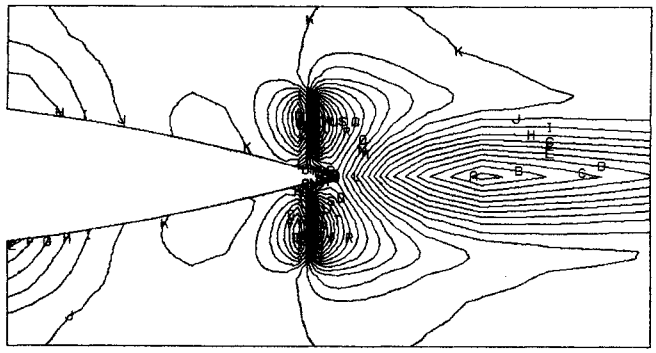

Legend A = −0.109 K = −0.004 V = −0.134
F = −0.051 P = −0.064 Z = −0.180

Fig. 3 Predicted baseline pressure contours in longitudinal section.

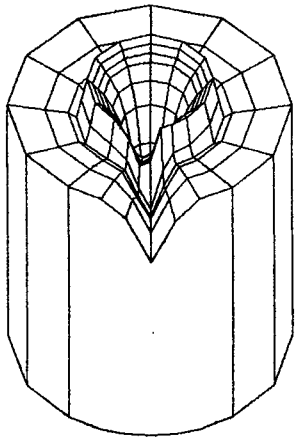

Fig. 4 Predicted baseline axial velocity surface plot at $X/D_0 = 0.208$.

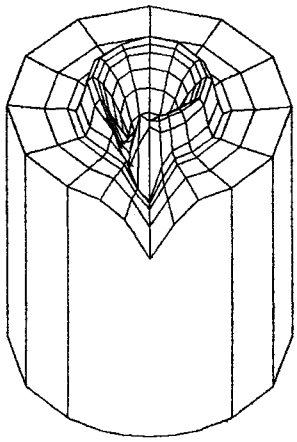

Fig. 5 Predicted baseline axial velocity surface plot at $X/D_0 = 1$.

Computational Strategy

The baseline case was solved by two successive substitution iterations followed by four quasi-Newton steps. The initial flowfield was obtained from an axisymmetric nonswirling flow analysis.

The overthrust case proved more difficult to solve. Successful convergence was achieved after three successive substitution steps followed by five quasi-Newton iterations.

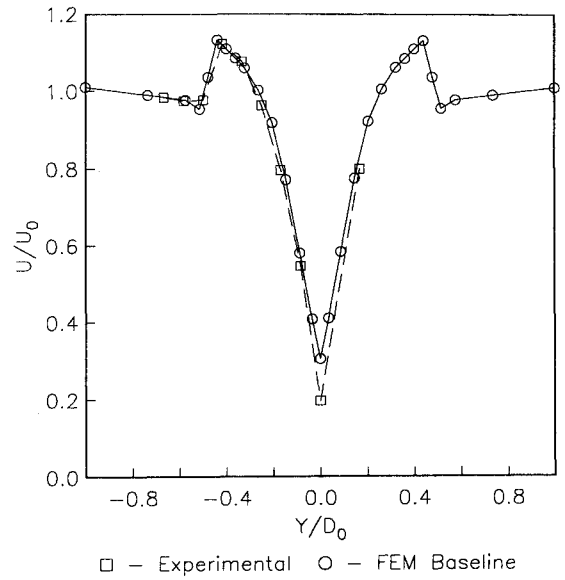

Fig. 6 Baseline prediction to experiment comparison of axial velocity, U vs Y at $X/D_0 = 0.208$.

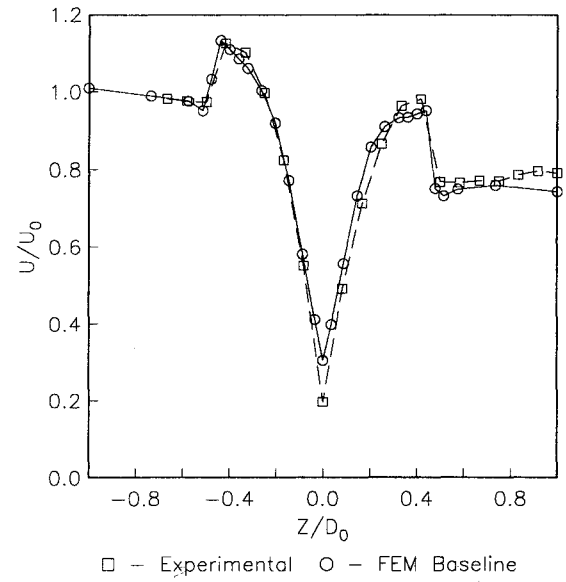

Fig. 7 Baseline prediction to experiment comparison of axial velocity, U vs Z at $X/D_0 = 0.208$.

Finally, the no-swirl case was easily solved in three quasi-Newton steps starting from an axisymmetric flowfield.

The global matrix contained 15,480 equations and required 370 Mbytes of storage for the 22,582,368 matrix coefficients. Calculations were performed on the Virginia Tech IBM-3084 computer. A summary of computing times and cost is given in Table 1.

Figure 3 shows pressure contours for the baseline configuration. The rapid variations of pressure due to the propeller are clearly seen. Pressure relaxation downstream of the propeller is evident. In fact, there seems to be a slight undershoot about 1 diameter downstream of the propeller. This effect is more pronounced here than observed by Pelletier and Schetz.[10,15] This is likely due to the higher propeller loading of the present case and to the presence of the body.

Surface plots of axial velocity, Figs. 4 and 5, clearly illustrate the development of the flow and the effect of the propeller on the wake of the strut. One can see the transport of the wake in the peripheral direction in the core region. The freestream ($r \geq 0.5$) remains unaffected by the propeller.

Comparison of Figs. 4 and 5 shows the effect of turbulent diffusion, which tends to smooth most of the sharp features

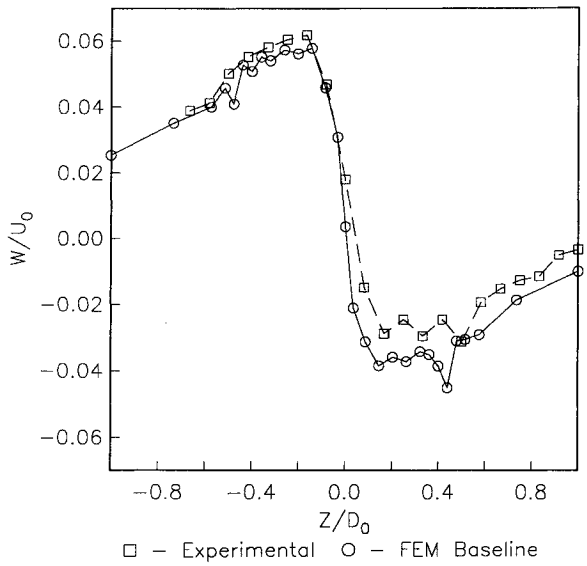

Fig. 8 Baseline prediction to experiment comparison of axial velocity, W vs Z at $X/D_0 = 0.208$.

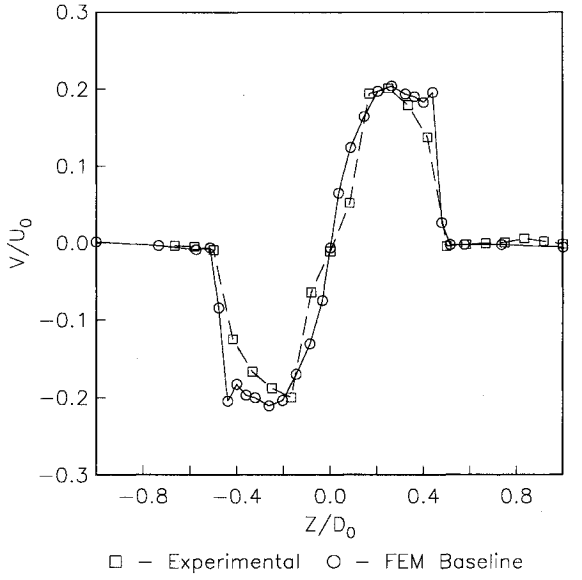

Fig. 9 Baseline prediction to experiment comparison of swirl velocity, V vs Z at $X/D_0 = 0.208$.

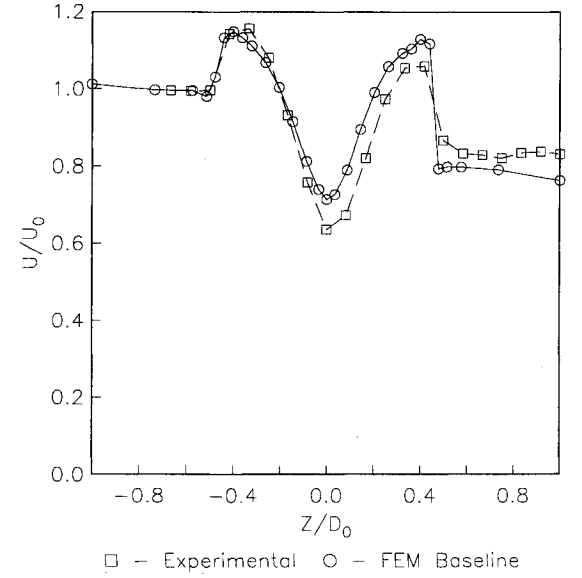

Fig. 10 Baseline prediction to experiment comparison of axial velocity, U vs Z at $X/D_0 = 1$.

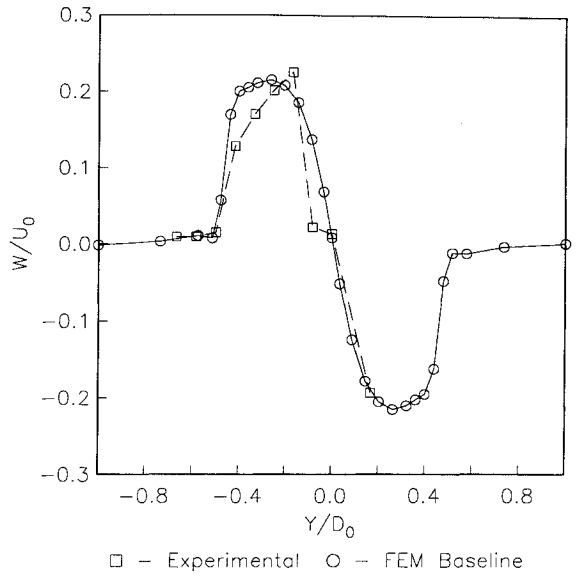

Fig. 11 Baseline prediction to experiment comparison of swirl velocity, W vs Y at $X/D_0 = 1$.

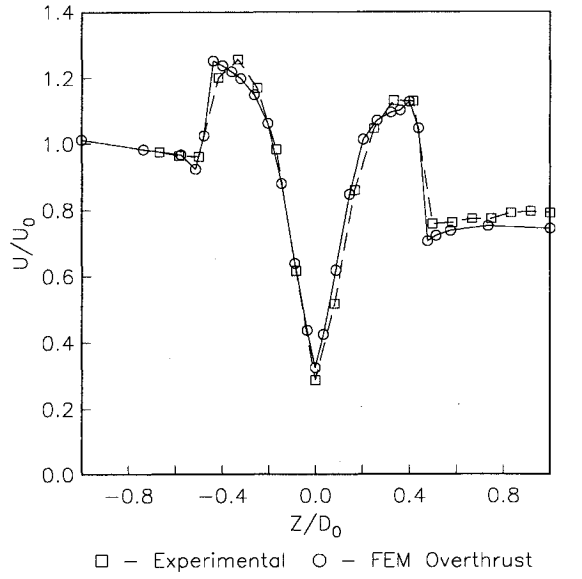

Fig. 12 Overthrust prediction to experiment comparison of axial velocity, U vs Z at $X/D_0 = 0.208$.

seen in Fig. 4. Note also the small velocity defect near the tip of the propeller, which is characteristic of the ring vortex of actuator disk theory and of real propellers.

Figures 6–11 show detailed comparison of predictions and experimental measurements. The predictions of axial velocity are in excellent agreement with experiments especially for the peaks of the profiles. The centerline velocity prediction is not nearly as good. This is an expected consequence due to the simplified treatment of the wall boundary layer. Similar agreement is observed for the vertical traverse.

Note that the small tip velocity defect documented in Refs. 15 and 33 is not seen in the experimental measurement. This could be attributed to the coarse distribution of experimental points, which can likely conceal the presence of the ring vortex.

Radial velocity predictions are excellent (see Fig. 8) even near the domain boundary. Predictions of swirl are the best known to the authors for this type of flow. It is interesting to note that swirl is unaffected by the planar wake as evidenced by the symmetric profiles in Figs. 9 and 11. However, the shape of the experimentally observed swirl profiles is more rounded than the predicted ones, indicating that the assumed

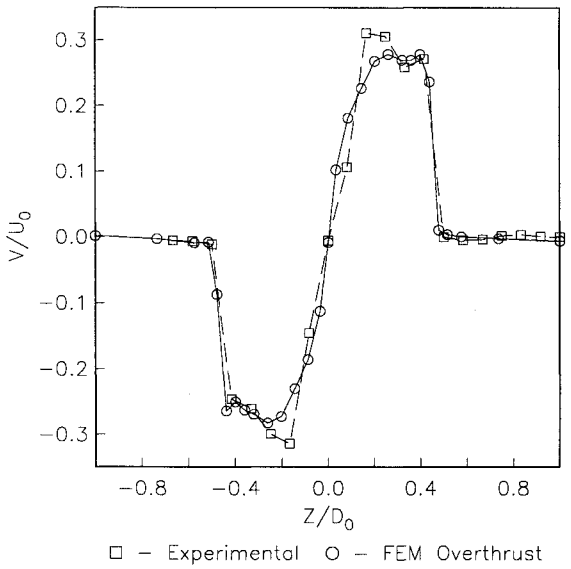

Fig. 13 Overthrust prediction to experiment comparison of swirl velocity, V vs Z at $X/D_0 = 0.208$.

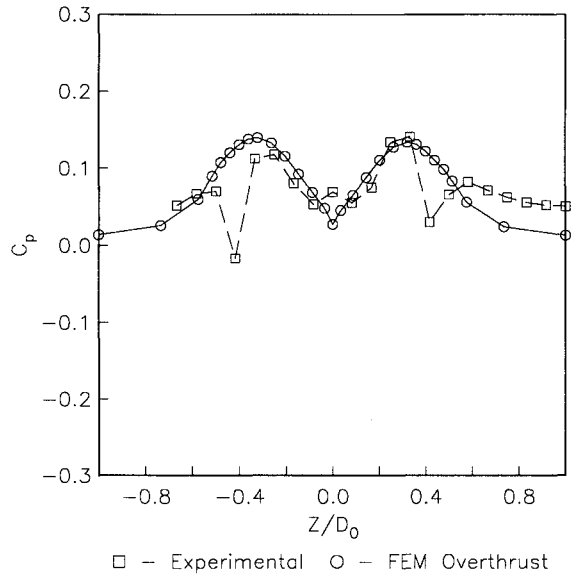

Fig. 14 Overthrust prediction to experiment comparison C_p at $X/D_0 = 0.208$.

distribution of swirl body force could be improved. Nevertheless, results are very good.

Figures 10 and 11 present comparisons at a station located $1D$ downstream of the propeller. Again, peaks are well predicted except in the strut wake. In general, the accuracy of prediction is somewhat lower than at the previous station. The radial velocity has decreased to less than 3% of the freestream so that both simulations and measurements had difficulty in producing smooth profiles.

Overthrust Configuration

Due to the 100% higher level of thrust, the features of the overthrust case are greatly accentuated as compared to the baseline solution. The upstream influence of the propeller at overthrust is greater than in the baseline case creating a peak velocity of 1.05 as compared to 1.02 at $X/D_0 = -0.5$. Peak swirl levels are 30% higher than those observed in the baseline configuration. Radial velocity peaks are 50% greater. Higher entrainment results from the increased thrust.

Comparisons of overthrust experiments to predictions along the vertical cut at $X/D_0 = -0.208$ are shown in Figs. 12 and 13. The axial velocity comparisons are even better than for the baseline case. The deficit of the planar wake is slightly under-

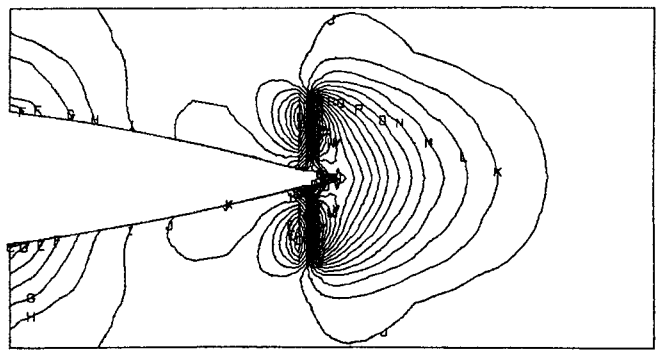

Legend A = −0.089 J = −0.009 T = −0.120
E = −0.045 P = −0.076 Z = −0.186

Fig. 15 Predicted no-swirl pressure contours in the longitudinal section.

predicted again. While the magnitude of the velocity peak compares extremely well, the shape of the excess region is not exact, with the experimental profile being slightly more rounded. The swirl predictions show a slight overshoot, but these predictions should be viewed as very good for such a high propeller loading.

Finally, Fig. 14 shows the generally good agreement obtained for the pressure coefficient. It should be noted that the experimentally measured pressures show the effects of the individual blade tip vortices. These vortices are responsible for the sharp drop in pressure at a dimensionless radius of 0.4. The actuator disk modeling of the propeller is incapable of reproducing this phenomenon.

No-Swirl Configuration

The no-swirl case operates at the same thrust level as the baseline calculation but with no torque added to the flow. The effect is quite large on the flowfield as can be seen by comparing Fig. 15 for the no-swirl case with Fig. 3. The pressure field is very different, decreasing smoothly from the propeller face downstream. The relaxation of the pressure is rapid, as has been noticed before. This large effect on the pressure field, by the removal of swirl, demonstrates the engineering importance of calculations of this type. The calculations were done relatively easily, allowing an assessment of the validity of the concept quickly. The very different pressure field could very well reduce the signature of the wake. Comparisons with the self-propelled experiments show predictions for axial and radial velocities nearly as good as in the baseline calculation. The interaction of the swirl with the axial and radial components can also be better understood.

Conclusions

Three-dimensional turbulent flows around a slender, propeller-driven body with a slender planar appendage were calculated. The actual geometry of a realistic body, its boundary layer, the wake from the appendage, and propellers operating at high loadings resulted in a highly three-dimensional flow.

A relatively small computational domain was needed, despite the complexity of the flow. This was mostly due to the traction-free boundary conditions applied at the freestream boundary and at the outflow.

Overall, predictions of all velocity components were excellent. The axial velocity peaks are especially well captured. The small velocity deficit beyond the tip of the propeller was also well reproduced. Swirl predictions are probably the best made yet for this type of problem. Radial velocity predictions are good. However, the actuator disk model cannot account for the effects of tip vortices on the mean pressure, which are present in the experiments. The multilayer turbulence model was essential to the inclusion of all major features of this flow.

Finally, the flow for an ideal rotor-stator combination was simulated. Results show that there is a negligible effect of swirl

on the axial and radial velocity fields. However, the pressure field shows significant differences with much faster decay downstream of the propeller.

Acknowledgment

This research was supported by the Office of Naval Research.

References

[1]Schetz, J. A., "Injection and Mixing in Turbulent Flow," *Progress in Astronautics and Aeronautics,* Vol. 68, AIAA, New York, 1980.

[2]Schetz, J. A., Daffan, E. B., and Jakubowski, A. K., "Turbulent Wake Behind Slender Propeller-Driven Bodies at Angles of Attack," *AIAA Journal,* Vol. 16, No. 1, Jan. 1978, pp. 6–8.

[3]Swanson, R. C., Schetz, J. A., and Jakubowski, A. K., "Turbulent Wake Behind Slender Bodies Including Self-Propelled Configurations," Aerospace and Ocean Engineering, Virginia Polytechnic Inst. and State Univ., Blacksburg, VA, VPI-Aero-024, 1974.

[4]Chieng, C. C., Jakubowski, A. K., and Schetz, J. A., "Investigation of Turbulent Properties of the Wake Behind Self-Propelled Axisymmetric Bodies," Aerospace and Ocean Engineering Dept., Virginia Polytechnic Inst. and State Univ., Blacksburg, VA, VPI-Aero-025, 1974.

[5]Lin, J. T., Pao, Y. H., and Veenhuizen, S. D., "Turbulent Wake of a Propeller-Driven Slender Body in Stratified and Non-Stratified Flow," *Bulletin of the American Physical Society,* Vol. 18, 1974, p. 1484.

[6]Swean, T. F., and Schetz, J. A., "Flow about a Propeller-Driven Body in a Temperature Stratified Fluid," *AIAA Journal,* Vol. 17, No. 8, 1979, pp. 863–869.

[7]Schetz, J. A., and Stottmeister, H. D., "The Flowfield near the Propeller of a Self-Propelled Slender Body," Society of Naval Architects and Marine Engineers Propellers '81 Meeting, 1981.

[8]Gad-el-Hak, M., and Lin, J. T., "Turbulence Measurements in the Near Wake of a Self-Propelled Slender Body," Flow Research Co., Silver Spring, MD, Flow Research Rept. 89, 1978.

[9]Schetz, J. A., Lee, H., and Kong, F., "Measurements in the Near-Wake Region of a Slender, Self-Propelled Model at Pitch or Yaw," *Journal of Ship Research,* Vol. 27, No. 4, Dec. 1983, pp. 227–235.

[10]Pelletier, D. H., and Schetz, J. A., "Finite Element Navier-Stokes Calculation of 3D Turbulent Flow Near a Propeller," *AIAA Journal,* Vol. 24, No. 9, 1986, pp. 1409–1416.

[11]Schetz, J. A., and Favin, S., "Numerical Solution of a Body-Propeller Combination Flow Including Swirl and Comparison with Data," *Journal of Hydronautics,* Vol. 13, No. 2, April 1979, pp. 46–51.

[12]Schetz, J. A., and Favin, S., "Numerical Solution for the Near Wake of a Body with Propeller," *Journal of Hydronautics,* Vol. 11, No. 4, Oct. 1977, pp. 136–141.

[13]Schetz, J. A., and Figard, R. L., "Numerical Solution of the Flow Near the Rotor of a Horizontal-Axis Wind Turbine and Comparison with Data," AIAA Paper 80-0608, April 1980.

[14]Schetz, J. A., and Figard, R. L., "Numerical Solution of the Flow Near the Rotor of a Wind Turbine," *Journal of Energy,* Vol. 6, No. 2, 1982.

[15]Schetz, J. A., Pelletier, D. H., and Mallory, D. A., "Experimental and Numerical Investigation of a Propeller with Three-Dimensional Inflow," *Journal of Propulsion and Power,* Vol. 4, No. 4, 1989, pp. 341–349.

[16]Mitra, P. S., Neu, W. L., and Schetz, J. A., "Effect of a Free Surface on the Wake of a Self-Propelled Slender Body," Aerospace and Ocean Engineering Dept., Virginia Polytechnic Institute and State Univ., Blacksburg, VA, Rept. No. 153, Jan. 1986.

[17]Holland, S., Neu, W. L., and Schetz, J. A., Aerospace and Ocean Engineering Dept., Virginia Polytechnic Institute and State Univ., Blacksburg, VA, unpublished work, 1986.

[18]Kaplan, P., private communication, 1987.

[19]McCormick, B. W., *Aerodynamics, Aeronautics, and Flight Mechanics,* Wiley, New York, 1979.

[20]Engelman, M. S., "FIDAP: A Fluid Dynamics Analysis Program," *Adv. Eng. Soft.,* Vol. 4, 1982.

[21]Hasbani, Y., and Engelman, M. S., "Out of Core Solution of Linear Equations with a Non-Symmetric Coefficient Matrix," *Comp. and Fluids,* Vol. 7, 1979.

[22]Rodi, W., *Turbulence Models and Their Application in Hydraulics,* International Association for Hydraulic Research, Delft, the Netherlands, 1980.

[23]Cebici, T., and Bradshaw, P., "Momentum Transfer in Boundary Layers," Hemisphere, McGraw-Hill, New York, 1977.

[24]Sforza, P. M., Steiger, M. H., and Trentacoste, N., "Studies on Three-Dimensional Viscous Jets," *AIAA Journal,* Vol. 1, No. 5, 1966.

[25]McGuirk, J. J., and Rodi, W., "The Calculation of Three-Dimensional Free Jets," *Turbulent Shear Flows I,* Springer-Verlag, New York, 1979.

[26]Hinze, J. O., *Turbulence,* 2nd ed., McGraw-Hill, New York, 1975, p. 539.

[27]Schlicting, H., *Boundary Layer Theory,* 7th ed., McGraw-Hill, New York, 1979, p. 745.

[28]Launder, B. E., and Spalding, D. B., *Lecturers in Mathematical Models of Turbulence,* Academic, New York, 1972.

[29]Clauser, F. H., "The Turbulent Boundary Layer," *Advances in Applied Mechanics,* Vol. IV, Academic, New York, 1956.

[30]Launder, B. E., Morse, A., Rodi, W., and Spalding, D. B., "The Prediction of Free Shear Flows, A Comparison of the Performance of Six Turbulence Models," NASA Conference on Free Shear Flows, Langley Field, Hampton, VA, July 1972, p. 15.

[31]Prandtl, L., "Bemerkungen zur Theorie der freien Turbulenz," *Z. Angew. Meth. Mech.,* Vol. 22, 1942, pp. 241–243.

[32]Schetz, J. A., *Foundations of Boundary Layer Theory for Momentum, Heat, and Mass Transfer,* Prentice-Hall, Englewood Cliffs, NJ, 1984, p. 236.

[33]Kotb, M. A., and Schetz, J. A., "Measurements of 3-D Turbulent Flow Behind a Propeller in a Shear Flow," *AIAA Journal,* Vol. 24, No. 4, 1986, pp. 570–577.